Calculation of the Electrothermal Parameters Associated with a Current Flowing Through an HVDC Ground System

Disciplina: IT 306 – Tópicos em Sistemas de Energia Elétrica III

Aluno: Joaquim de Sousa Lima Neto

PURPOSE

To present a distinct formulation to represent the electrothermal phenomena associated with HVDC ring electrodes.

CONTENTS

1 – Introduction

2 – Electric Parameters

3 – Heat Conduction

4 – Finite Element Method

5 – Results

6 – Conclusions

7 - References

CONTENTS

1 – Introduction

INTRODUCTION

Quando usar Corrente Contínua em Alta Tensão – CCAT
(High Voltage Direct Current – HVDC)
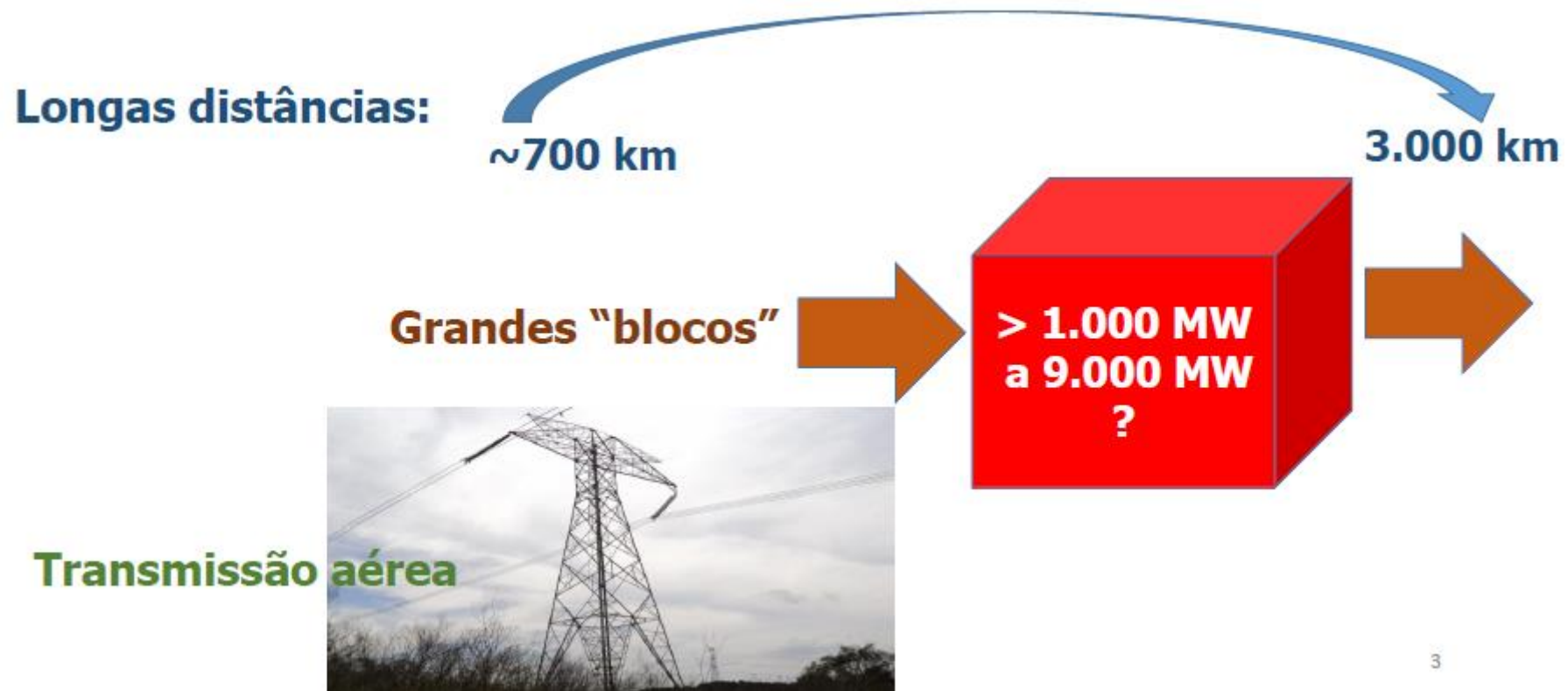
INTRODUCTION

- ✓ Travessia de rios, lagos e oceanos

- ✓ Conectar sistemas AC assíncronos

- ✓ Conectar sistemas de frequências diferentes

- ✓ Back-to-back

- ✓ Transmissão subterrânea por cabos

- ✓ Transmissão aérea em longas distâncias

6
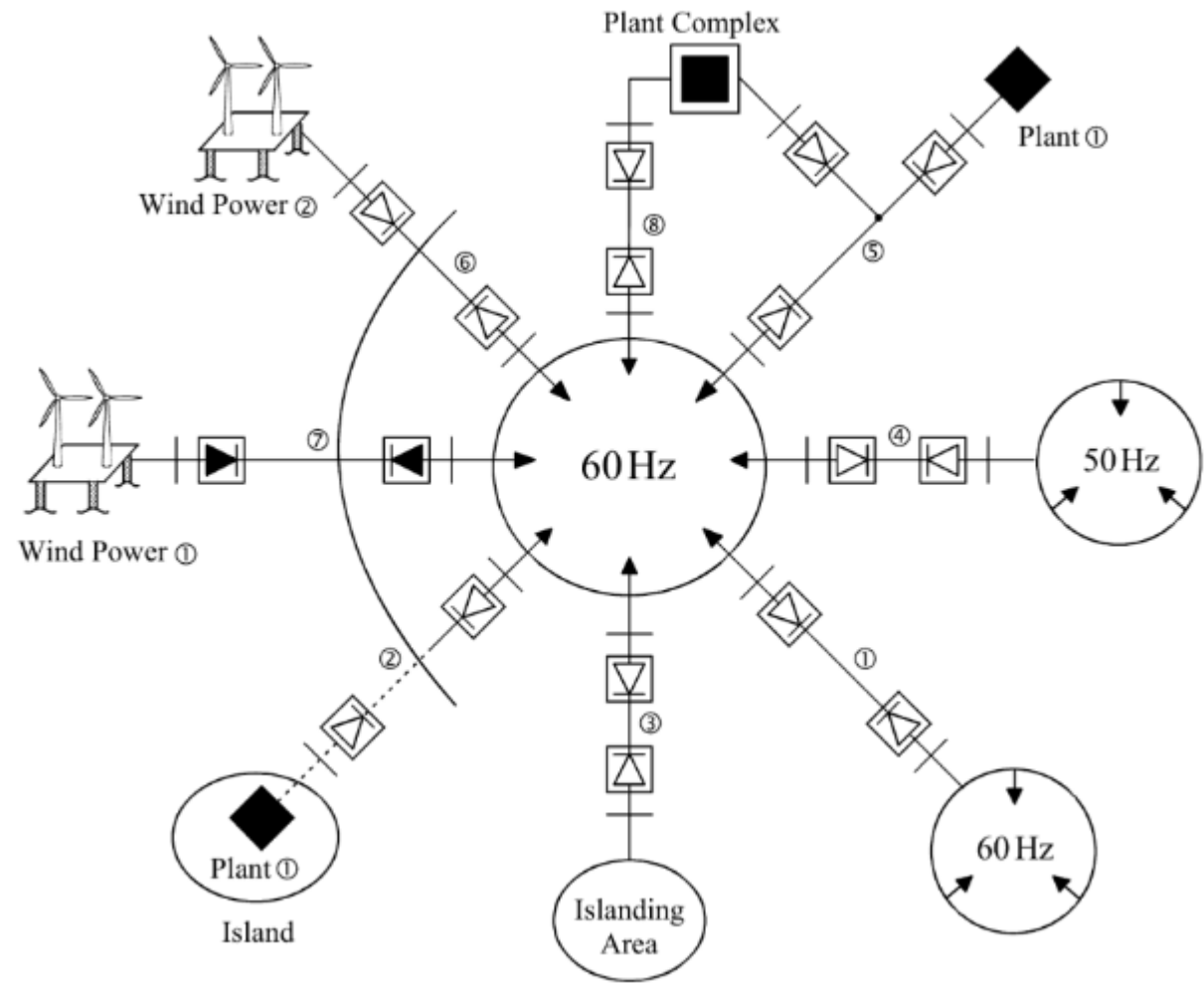
INTRODUCTION

Vantagens

✓ Maior potência por condutor

✓ Torres e linhas mais simples

✓ Pode usar retorno pela terra

✓ Sem efeito pelicular

✓ Sem corrente de carregamento

✓ Fator de potência unitário

✓ Menor impacto ambiental
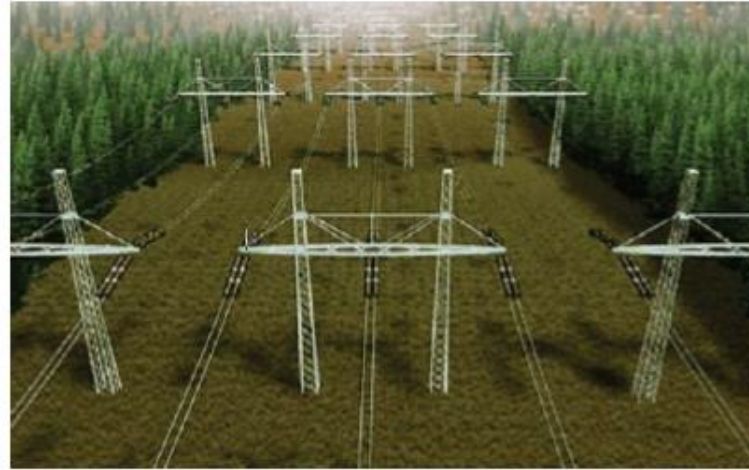
a) Corredor de transmissão CA 500 kV:
3 circuitos, capacidade 3.000 a 4.500 MW

b) Corredor de transmissão CC
Bipolo ± 500 kV, 3.000 MW

INTRODUCTION

Desvantagens

- ✓ Preço dos conversores

- ✓ Potência reativa requerida pelos conversores

- ✓ Os conversores geram harmônicos

- ✓ Não há disjuntor para operar em DC

INTRODUCTION

Linhas HVDC no Brasil

Figura 2.1: Potencial eólico (Região Nordeste)

Xingu-Estreito HVDC
± 800 kV, 2086 km, 4 GW (2017)

Rio Madeira HVDC
2x(± 600 kV), 2385 km,
2x3.15 GW (2013/14)

Xingu-T. Rio HVDC
± 800 kV, 2539 km,
4 GW (2019)

Itaipu HVDC
2x(± 600 kV), 810 km,
2x3.15 GW (1984/87)

Garabi
2000 MW

Uruguaiana
50 MW

Rivera
70 MW

Melo
500 MW
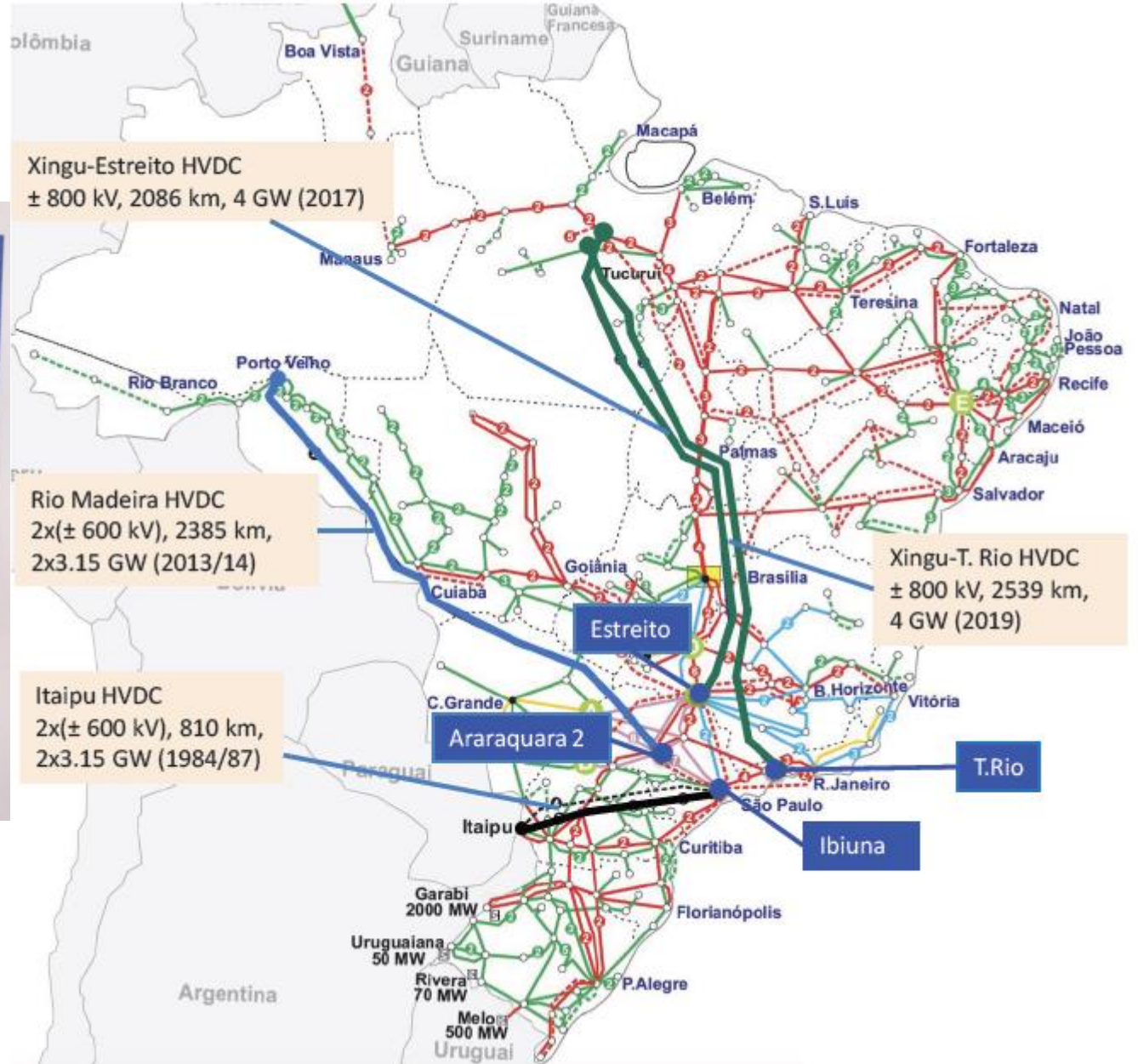
INTRODUCTION

**Ponto de Equilíbrio de Custos
CA/CC (break-even distance)**
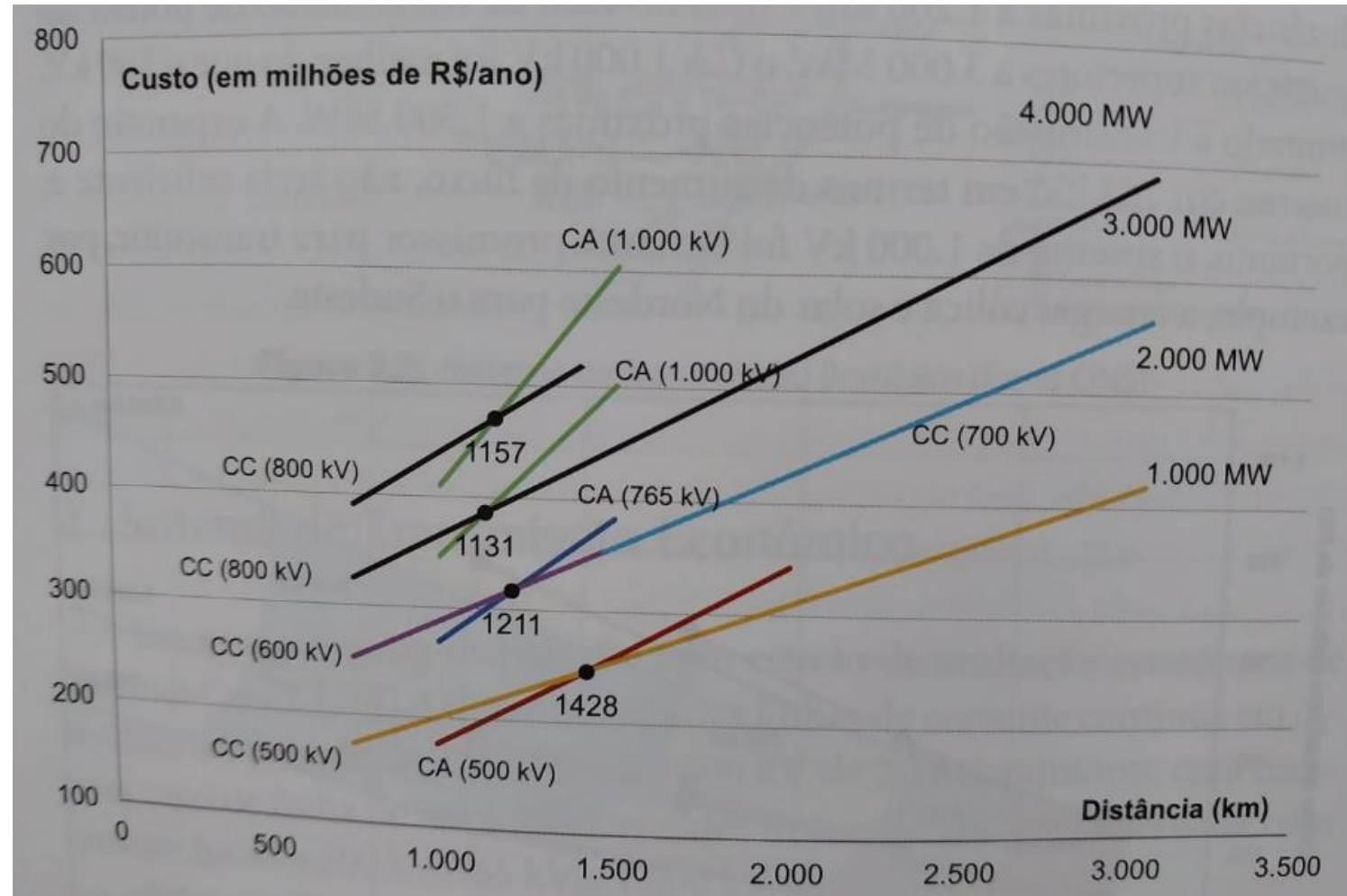
INTRODUCTION

Diagrama unifilar e modos de operação (Line-Commutated Current-sourced Converter – LCC ou CSC)
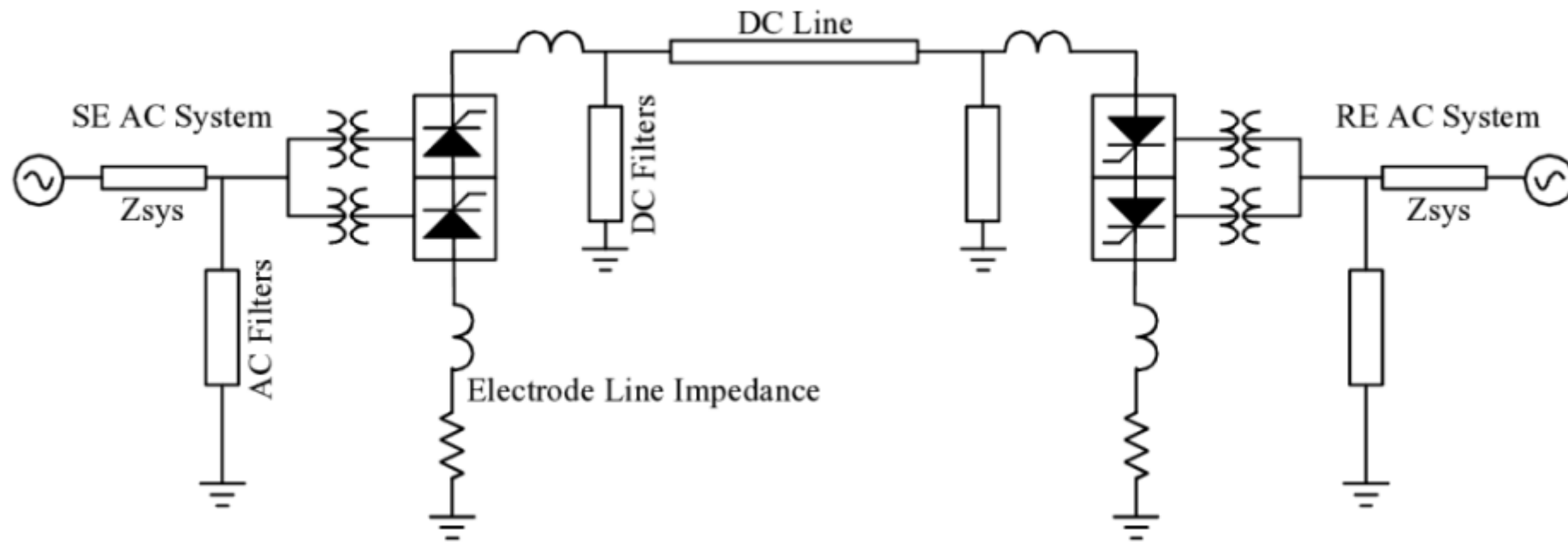
Operação Monopolar

INTRODUCTION

Diagrama unifilar e modos de operação
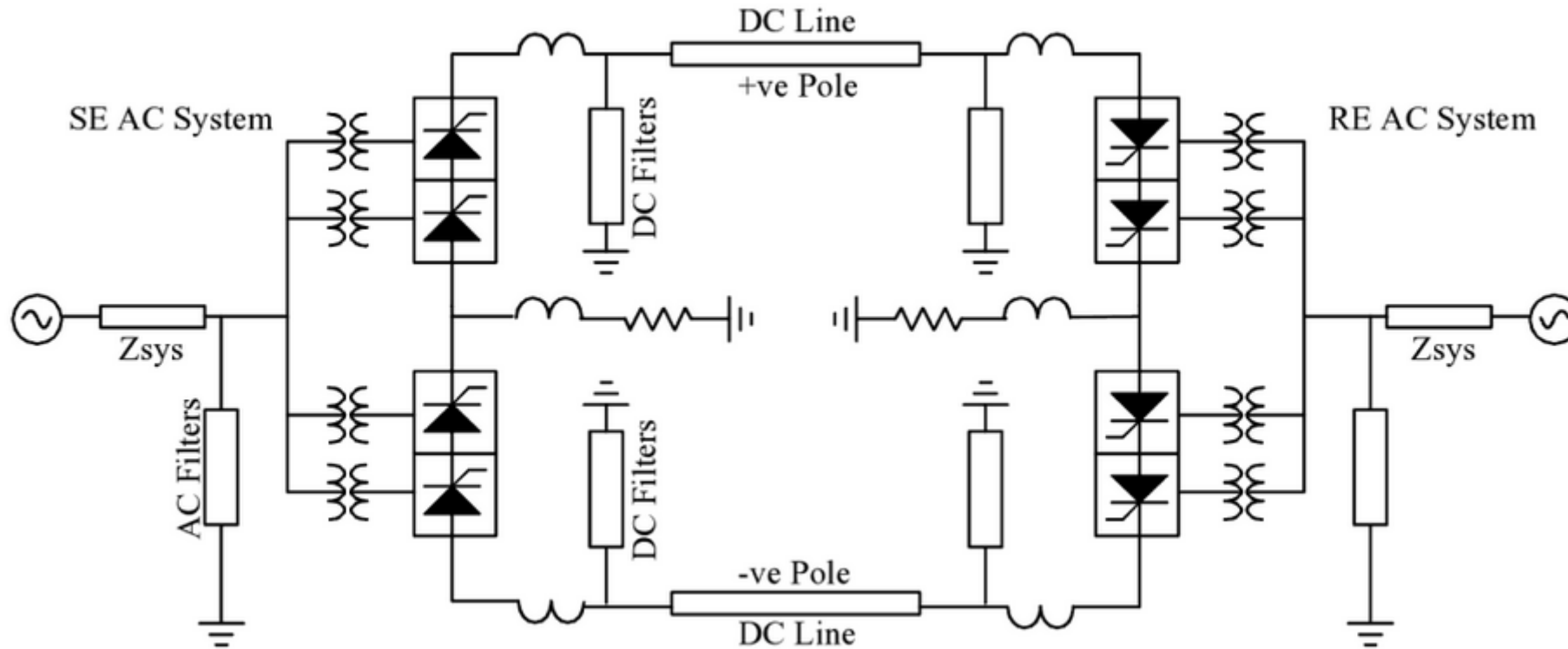
Operação Bipolar

INTRODUCTION

Diagrama unifilar real de um terminal
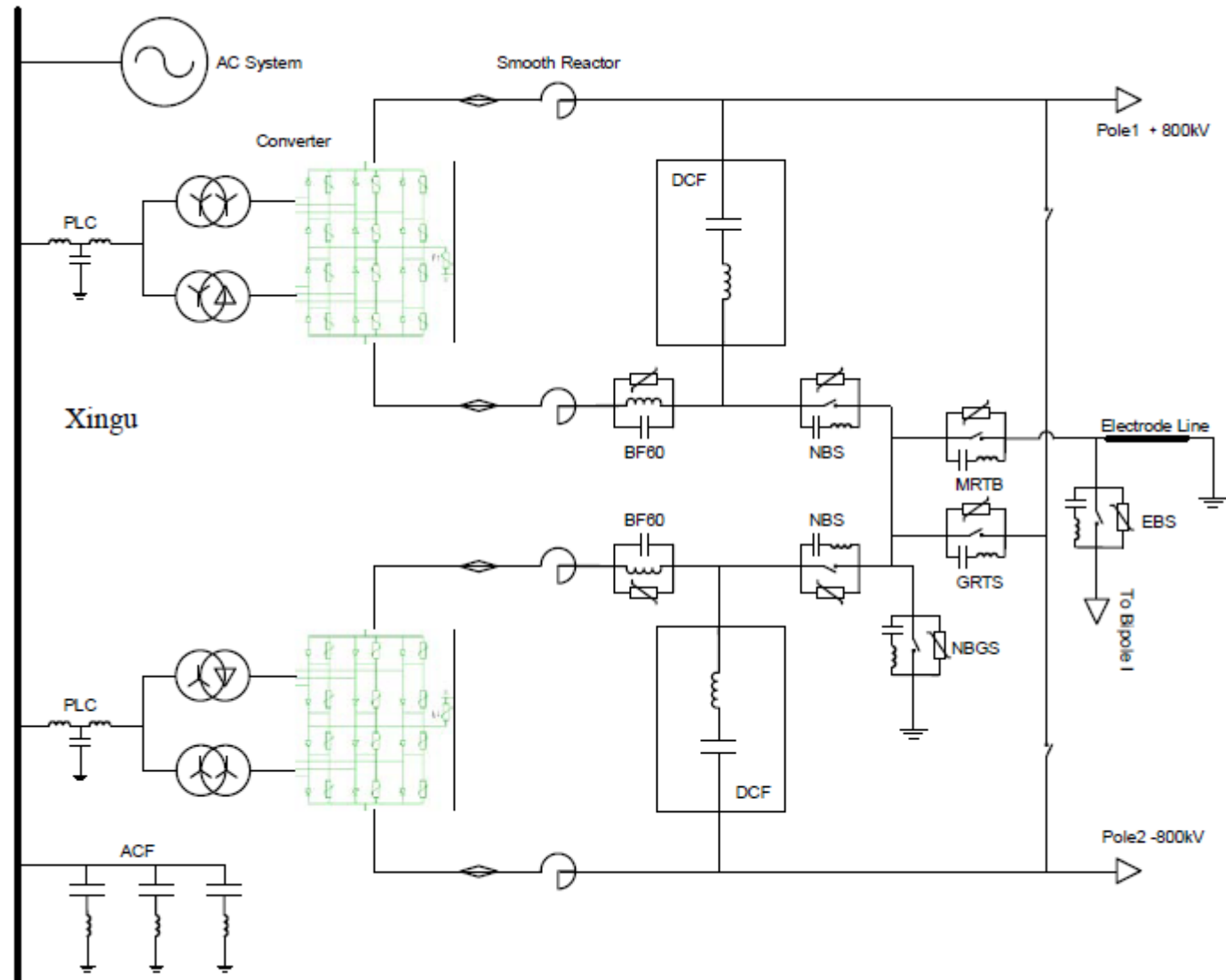
INTRODUCTION

Terminal Xingu
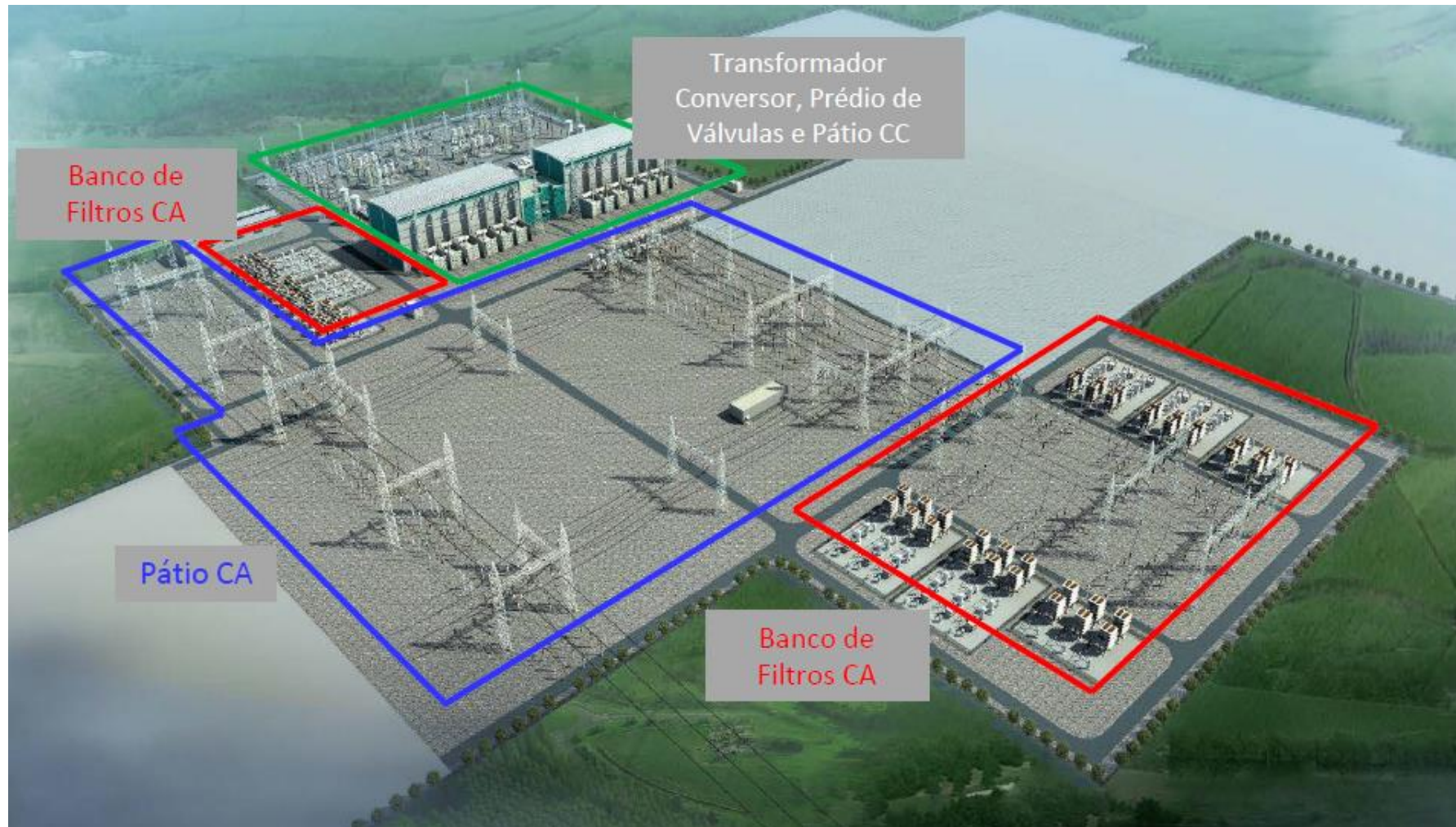
INTRODUCTION
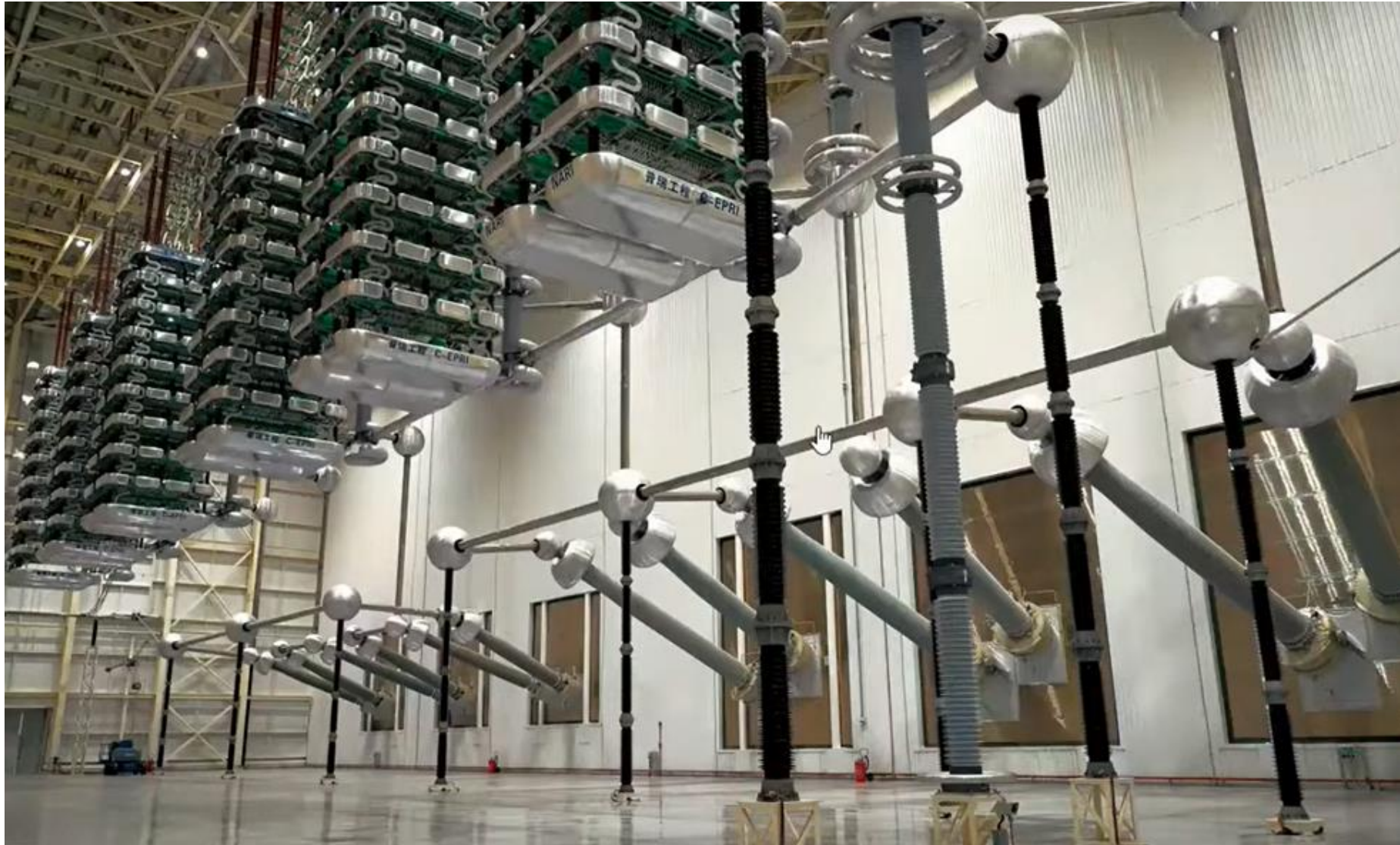
Terminal Xingu

INTRODUCTION
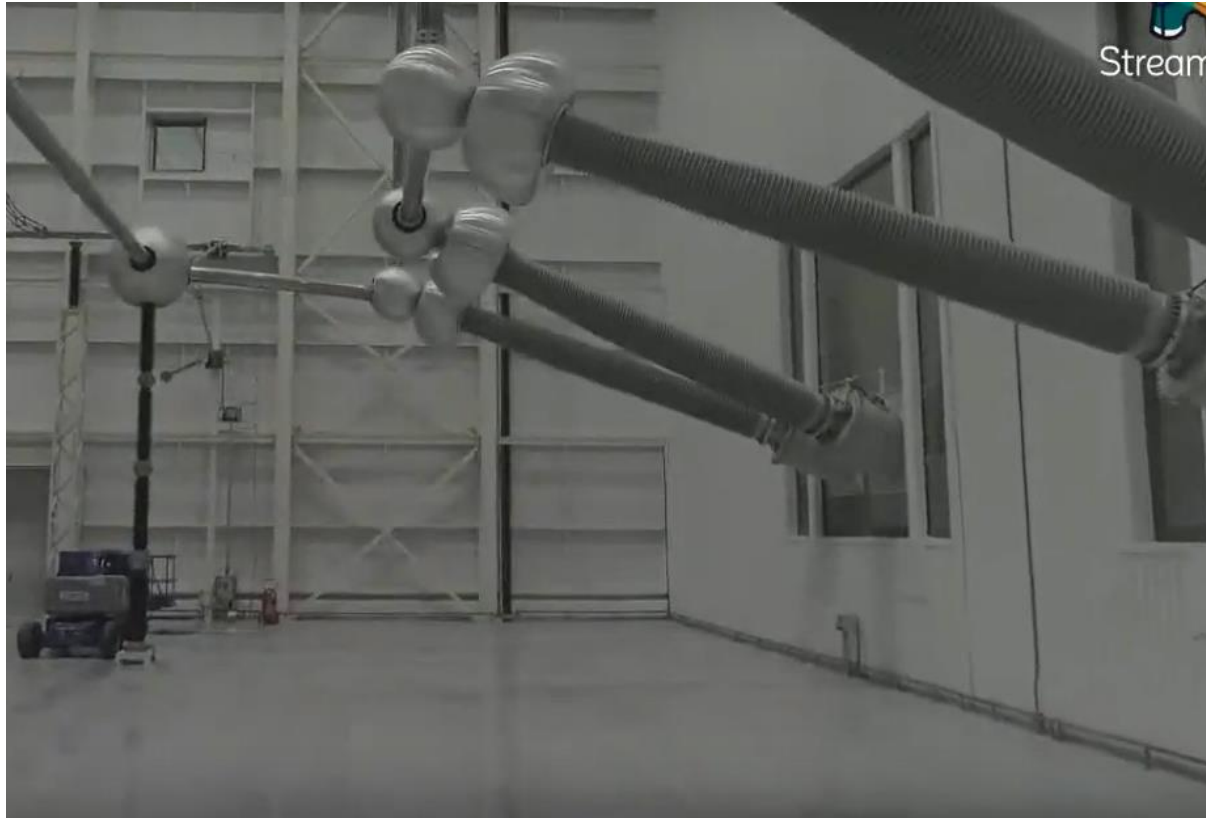
Terminal Xingu

INTRODUCTION

Terminal Xingu

INTRODUCTION

Terminal Xingu

- ✓ Eletrodo de aterramento do bipolo a 38 km da SE Xingu

- ✓ 600 metros de diâmetro

- ✓ 3,5m de profundidade

Linha que conecta a SE ao eletrodo

INTRODUCTION

- An HVDC system is composed of converter (rectifier and inverter) stations, transmission lines, and ground electrodes or metallic return.

- A monopolar operation with ground return may conduct thousands of amperes for long periods of time, such as several months. Thus, the correct design of HVDC ground electrodes is of the utmost importance.
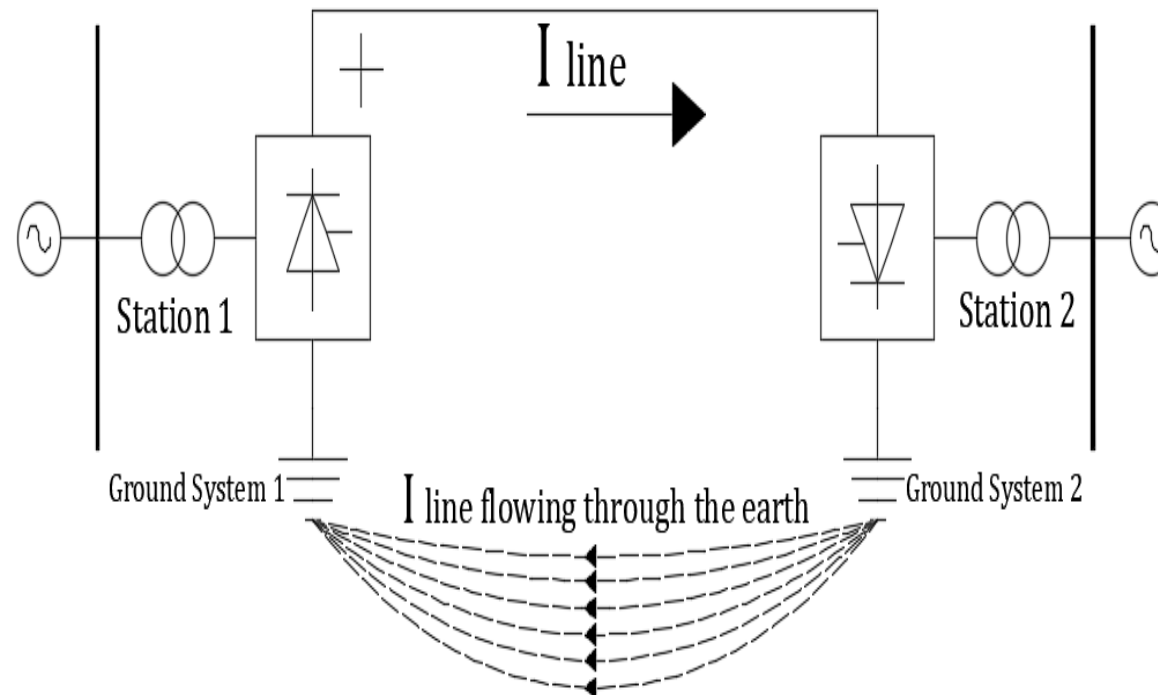
1 - Monopolar operation of an HVDC system

INTRODUCTION

- The physical and chemical properties of the soil are as important as the ground electrode geometry, which can have a ring, straight, or star form.

- The best layout must be chosen based on the available area and the type and stratification of the soil.

- Ring (or toroidal) electrodes spread the current more uniformly in a homogeneous soil, thus it is the most common type. This is the electrode form chosen for this paper.

CONTENTS

ELECTRIC PARAMETERS

Let's consider the linearly charged ring electrode represented below, with a uniform charge density λ (in C/m), to calculate the electric potential *V* with respect to remote earth.
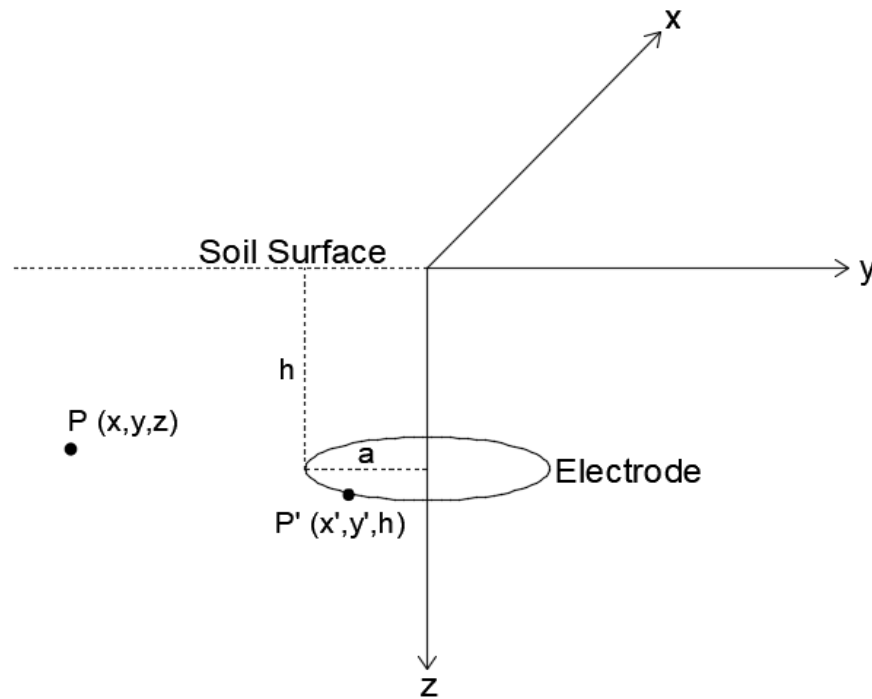
2 - Tridimensional representation of the toroidal electrode
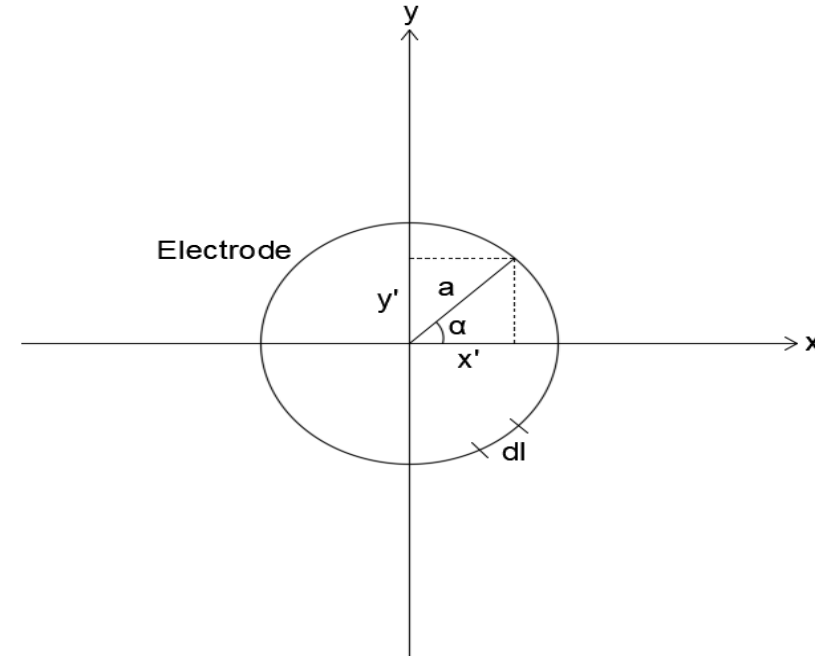
3 - Upper view

ELECTRIC PARAMETERS

The potential *V* at an arbitrary point *P(x,y,z)* due to a linear charge distribution can be found using Coulomb's or Gauss' Law, as shown by Equation 1.

$$V(x,y,z) = \frac{1}{4\pi\varepsilon}\int \frac{\lambda\,dl}{|P-P'|} \qquad (1)$$

ε is soil permittivity
P is an arbitrary point in the surroundings
P' is an arbitrary source point in the circumference
dl is a differential element of the circumference, given by $dl = a.d\alpha$
$|P-P'|$ is the magnitude of the distance from *P* to *P'*.
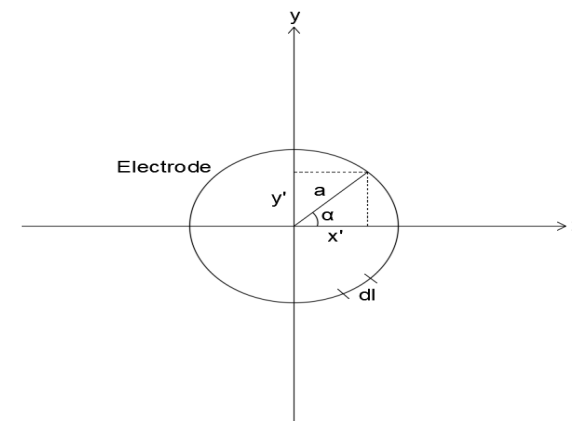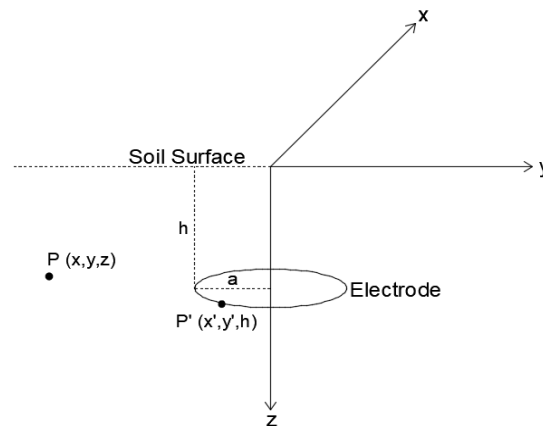
ELECTRIC PARAMETERS

In cylindrical coordinates

$$P(x, y, z) = P(r \cos\varphi, r \sin\varphi, z)$$

$$P'(x, y, h) = P'(a \cos\alpha, a \sin\alpha, h)$$

$$r = \sqrt{x^2 + y^2}, \; \cos\varphi = \frac{x}{r} \text{ and } \sin\varphi = \frac{y}{r}$$

then $P - P'$ can be written as

$$P - P' = (r \cos\varphi - a \cos\alpha)\boldsymbol{ax} + (r \sin\varphi - a \sin\alpha)\boldsymbol{ay} + (z - h)\boldsymbol{az} \quad (2)$$

where *ax*, *ay* and *az* are unit vectors along axes *x, y* and *z* respectively, which can be related to cylindrical coordinates by the following equation:

$$ax = \cos\varphi \; ar - \sin\varphi \; a\varphi \qquad (3)$$

$$ay = \sin\varphi \; ar + \cos\varphi \; a\varphi \qquad (4)$$

ELECTRIC PARAMETERS

After some algebraic manipulation we obtain the following:

$$P - P' = [r - a\cos(\alpha - \varphi)]\, ar - a\sin(\alpha - \varphi)a\varphi + (z - h)az \quad (5)$$

$$|P - P'| = \sqrt{[r - a\cos(\alpha - \varphi)]^2 + [-a\sin(\alpha - \varphi)]^2 + (z - h)^2} \quad (6)$$

From the electromagnetic theory, we know the following to be true:

$$i = \oint J.\,ds \qquad (7)$$

$$J = \frac{E}{\rho} \qquad (8)$$

$$E = \frac{D}{\varepsilon} \qquad (9)$$

$$\lambda = \frac{Q}{2\pi a} \qquad (10)$$

$$Q = \oint D.\,ds \qquad (11)$$

Replacing (8), (9), (10) and (11) in (7) leads to

$$i = \oint \frac{D}{\rho\varepsilon}.\,ds = \frac{1}{\rho\varepsilon}\oint D.\,ds \rightarrow i = \frac{Q}{\rho\varepsilon} \rightarrow \boldsymbol{i = \frac{2\pi a\lambda}{\rho\varepsilon}} \qquad (12)$$

Then equation 12 can be written as:

$$\boldsymbol{i = \frac{2\pi a\lambda}{\rho\varepsilon}} \rightarrow \frac{\lambda a}{\varepsilon} = \frac{\rho i}{2\pi} \qquad (12)$$

ELECTRIC PARAMETERS

$$V(x, y, z) = \frac{1}{4\pi\varepsilon} \int \frac{\lambda \, dl}{|P - P'|} \qquad (1)$$

$$|P - P'| = \sqrt{[r - a\cos(\alpha - \varphi)]^2 + [-a\sin(\alpha - \varphi)]^2 + (z - h)^2} \qquad (6)$$

By using (6) in (1) and rewriting it in cylindrical coordinates we obtain

$$V(r, \varphi, z) = \frac{\lambda \, a}{4\pi\varepsilon} \int_0^{2\pi} \frac{d\alpha}{\sqrt{[r - a\cos(\alpha - \varphi)]^2 + [-a\sin(\alpha - \varphi)]^2 + (z - h)^2}} \qquad (13)$$

Substituting (12) in (13) it results in the following:

$$V(r, \varphi, z) = \frac{\rho i}{8\pi^2} \int_0^{2\pi} \frac{d\alpha}{\sqrt{[r - a\cos(\alpha - \varphi)]^2 + [-a\sin(\alpha - \varphi)]^2 + (z - h)^2}} \qquad (14)$$

ELECTRIC PARAMETERS

$$V(r, \varphi, z) = \frac{\rho i}{8\pi^2} \int_0^{2\pi} \frac{d\alpha}{\sqrt{[r - a\cos(\alpha - \varphi)]^2 + [-a\sin(\alpha - \varphi)]^2 + (z - h)^2}} \tag{14}$$

- Equation 14 represents the electric potential in the vicinities of the toroid placed at $z = h$.

- To satisfy the boundary conditions at the air-soil interface ($z = 0$), we must assume that a second electrode is placed at $z = -h$. This procedure is known as the Method of Images. Thus, the electrical parameters V, E and J are calculated by the superposition of the two electrodes.

- By means of the same method used to deduce (14), the potential due to the imaginary toroid (placed at $z = -h$) is as follows:

$$V(r, \varphi, z) = \frac{\rho i}{8\pi^2} \int_0^{2\pi} \frac{d\alpha}{\sqrt{[r - a\cos(\alpha - \varphi)]^2 + [-a\sin(\alpha - \varphi)]^2 + (z + h)^2}} \tag{15}$$

27

ELECTRIC PARAMETERS

Thus, the electric potential, due to the two conductors, becomes the equation below:

$$V(r, \varphi, z) = \frac{\rho i}{8\pi^2} \int_0^{2\pi} \frac{d\alpha}{\sqrt{[r - a\cos(\alpha - \varphi)]^2 + [-a\sin(\alpha - \varphi)]^2 + (z - h)^2}}$$

$$+ \frac{\rho i}{8\pi^2} \int_0^{2\pi} \frac{d\alpha}{\sqrt{[r - a\cos(\alpha - \varphi)]^2 + [-a\sin(\alpha - \varphi)]^2 + (z + h)^2}} \qquad (16)$$

By using this equation, it can be noticed that *V* does not change along the *φ*-direction, which was expected because of the symmetry of the electrode. In other words, equation 16 can be simplified if we consider *φ = 0*, which becomes, considering only two dimensions (*r* and *z*), the following:

$$V(r, z) = \frac{\rho i}{8\pi^2} \left[\int_0^{2\pi} \frac{d\alpha}{\sqrt{[r - a\cos(\alpha)]^2 + a^2\sin^2\alpha + (z - h)^2}} + \int_0^{2\pi} \frac{d\alpha}{\sqrt{[r - a\cos(\alpha)]^2 + a^2\sin^2\alpha + (z + h)^2}} \right] \qquad (17)$$

ELECTRIC PARAMETERS

$$V(r,z) = \frac{\rho i}{8\pi^2}\left[\int_0^{2\pi} \frac{d\alpha}{\sqrt{[r-a\cos(\alpha)]^2 + a^2\sin^2\alpha + (z-h)^2}} + \int_0^{2\pi} \frac{d\alpha}{\sqrt{[r-a\cos(\alpha)]^2 + a^2\sin^2\alpha + (z+h)^2}}\right] \quad (17)$$

The solution for equation 17 is expressed by elliptic integrals of the first kind, as shown below from the Mathematica programming language.

$$V[r\_, z\_] = \frac{i\,\rho\left(\dfrac{\text{EllipticK}\left[-\dfrac{4\,a\,r}{(a-r)^2+(h-z)^2}\right]}{\sqrt{(a-r)^2+(h-z)^2}} + \dfrac{\text{EllipticK}\left[-\dfrac{4\,a\,r}{(a-r)^2+(h+z)^2}\right]}{\sqrt{(a-r)^2+(h+z)^2}}\right)}{2\,\pi^2}$$

With equation 17 and considering the electromagnetic theory, we can also obtain E and J in the r- and z-direction, which are related to V by the following equations:

$$Er = -\frac{\partial V_{eletrodo}(r,z)}{\partial r} \quad (18) \qquad\qquad Jr = \frac{Er}{\rho} \quad (21)$$

$$Ez = -\frac{\partial V_{eletrodo}(r,z)}{\partial z} \quad (19) \qquad\qquad Jz = \frac{Ez}{\rho} \quad (22)$$

$$E(r,z) = \sqrt{Er^2 + Ez^2} \quad (20) \qquad\qquad J(r,z) = \sqrt{Jr^2 + Jz^2} \quad (23)$$

CONTENTS

HEAT CONDUCTION

The general heat conduction equation in cylindrical coordinates is given by

$$\frac{1}{r}\frac{\partial}{\partial r}\left(k\, r\, \frac{\partial T}{\partial r}\right) + \frac{1}{r^2}\frac{\partial}{\partial \varphi}\left(k\, \frac{\partial T}{\partial \varphi}\right) + \frac{\partial}{\partial z}\left(k\, \frac{\partial T}{\partial z}\right) + g = de.\, C\, \frac{\partial T}{\partial t} \qquad (24)$$

where

r, φ and z are the cylindrical coordinates

k is the thermal conductivity in W/$^\circ$C.m

g is the heat generated by the Joule effect in W/m³

de is the soil density in kg/m³

C is the specific heat in J/(kg.$^\circ$C)

T is the temperature in $^\circ$C

t is the time in seconds

Considering an isotropic and homogeneous soil and no variation in the φ-direction, equation 24 can be reduced to

$$\frac{\partial^2 T}{\partial r^2} + \frac{1}{r}\frac{\partial T}{\partial r} + \frac{\partial^2 T}{\partial z^2} + \frac{g}{k} = \frac{1}{\alpha}\frac{\partial T}{\partial t} \qquad (25)$$

HEAT CONDUCTION

$$\frac{\partial^2 T}{\partial r^2} + \frac{1}{r}\frac{\partial T}{\partial r} + \frac{\partial^2 T}{\partial z^2} + \frac{\rho.J^2}{k} = \frac{1}{\alpha}\frac{\partial T}{\partial t} \qquad (25)$$

where

$$g = \rho.J^2$$

$\alpha = \dfrac{k}{de.C}$ is the thermal diffusivity (m²/s)

The formulation presented in (25) is commonly known as the Fourier-Biot equation.

HEAT CONDUCTION

$$\frac{\partial^2 T}{\partial r^2} + \frac{1}{r}\frac{\partial T}{\partial r} + \frac{\partial^2 T}{\partial z^2} + \frac{\rho.J^2}{k} = \frac{1}{\alpha}\frac{\partial T}{\partial t} \qquad (25)$$

Boundary Conditions

$(a)\ T(t,r,z) = Temperature\ at\ a\ given\ time\ and\ space$

$(b)\ T(0,r,z) = T_{ini} = T_{air}$

$(c)\ T(t,r_1,z) = T(t,r_2,z) = T(t,r,z_2) = T_{ini}$

$(d)\ \dfrac{\partial T(t,r,z_0)}{\partial z} = \dfrac{h_c}{k}[\ T(t,r,z_0) - T_{air}]$

where

T_{ini} = temperature (°C) at $t = 0$
T_{air} = air temperature (°C)
r_1 = remote point from the electrode at the negative direction of r (m)
r_2 = remote point from the electrode at the positive direction of r (m)
z_0 = soil surface, i.e. $z = 0$
z_2 = remote point from the electrode at the positive direction of z, i.e. far from the soil surface
h_c = convection heat transfer coefficient (W/°C.m²)

CONTENTS

FINITE ELEMENT METHOD

$$\frac{\partial^2 T}{\partial r^2} + \frac{1}{r}\frac{\partial T}{\partial r} + \frac{\partial^2 T}{\partial z^2} + \frac{\rho . J^2}{k} = \frac{1}{\alpha}\frac{\partial T}{\partial t} \qquad (25)$$

In order to solve equation 25 using the finite element method, the Mathematica programming language was used, in which a rectangular area near the electrode was chosen, as shown in Figure 4.
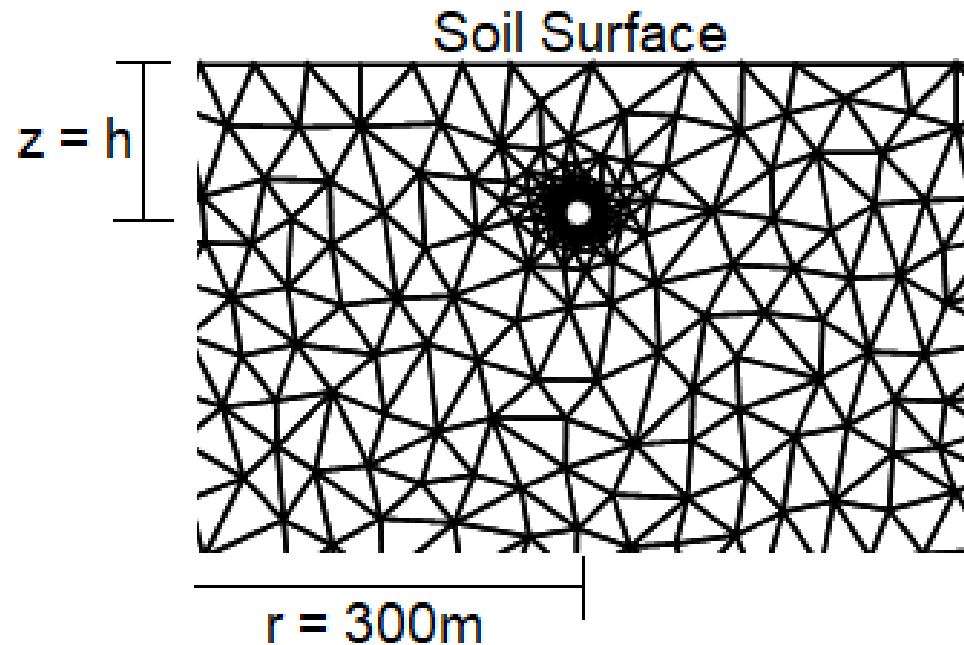
Figure 4 – Mesh representation of the soil near the electrode

FINITE ELEMENT METHOD

It was verified that the smaller the triangle length, the more computational time was required to solve the differential equation, but the results would remain the same, showing that the solution had converged.
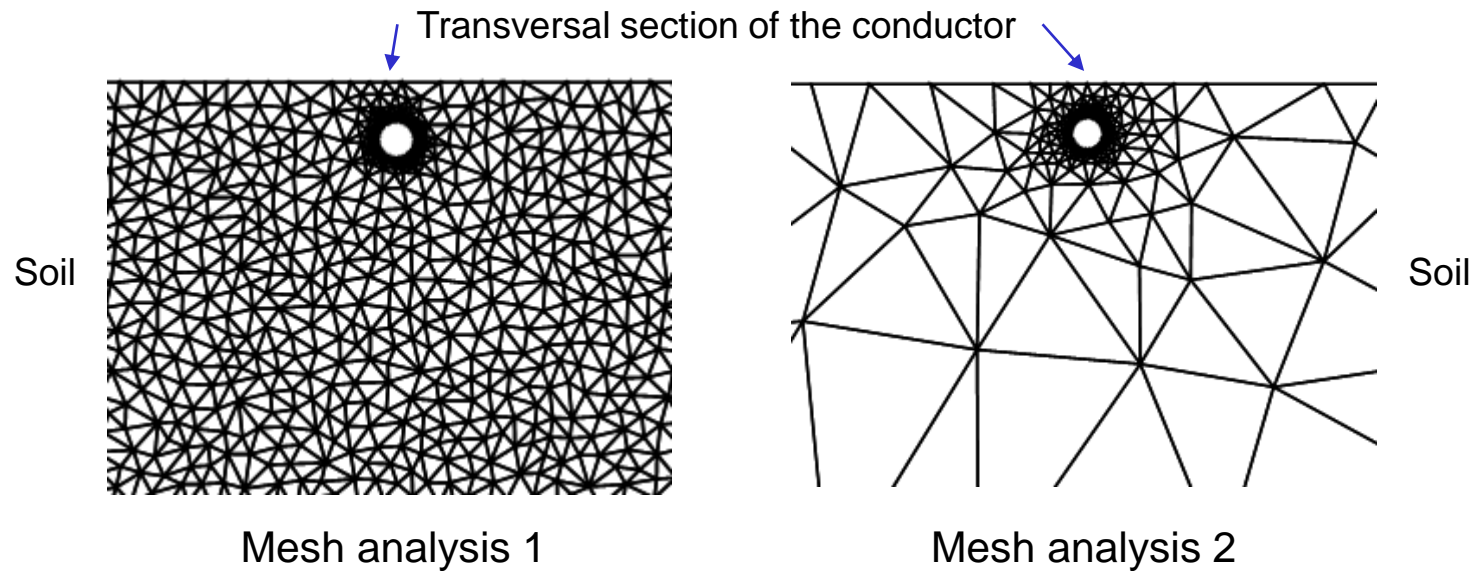
Transversal section of the conductor

Soil

Soil

Mesh analysis 1

Mesh analysis 2

CONTENTS

1 – Introduction

2 – Electric Parameters

3 – Heat Conduction

4 – Finite Element Method

5 – Results

6 – Conclusions

7 - References

RESULTS

The analyzed configuration is presented in Table I, shown below.

Toroidal radius	a = 300 m
Electrode section diameter	d = 0.6 m
Remote point at -r direction	r_1 = 260 m
Depth of burial	h = 2.7 m
Remote point at +r direction	r_2 = 340 m
Interface at soil surface	z_0 = 0
Remote point at +z direction	z_2 = 40 m
Injected current	i = 2000 A
Soil resistivity	ρ = 100 Ω.m
Thermal conductivities	k = 0.26, 2.6 and 4 W/°C.m
Thermal diffusivity	α = 7.74 x 10^{-7} m²/s
Initial soil temperature in °C	T_{ini} = 18°C
Convection heat transfer coefficient	h_c = 1 W/°C.m²
Air temperature	T_{air} = 18°C

RESULTS

By using Table 1 and Equations 17, 20, 23 and 25 we obtain the results given in Figures 5 to 13.

$$V(r,z) = \frac{\rho i}{8\pi^2}\left[\int_0^{2\pi} \frac{d\alpha}{\sqrt{[r - a\cos(\alpha)]^2 + a^2\sin^2\alpha + (z-h)^2}} + \int_0^{2\pi} \frac{d\alpha}{\sqrt{[r - a\cos(\alpha)]^2 + a^2\sin^2\alpha + (z+h)^2}}\right] \quad (17)$$

$$E(r,z) = \sqrt{Er^2 + Ez^2} \qquad (20)$$

$$J(r,z) = \sqrt{Jr^2 + Jz^2} \qquad (23)$$

$$\frac{\partial^2 T}{\partial r^2} + \frac{1}{r}\frac{\partial T}{\partial r} + \frac{\partial^2 T}{\partial z^2} + \frac{\rho.J^2}{k} = \frac{1}{\alpha}\frac{\partial T}{\partial t} \qquad (25)$$

RESULTS

$$V(r,z) = \frac{\rho i}{8\pi^2} \left[\int_0^{2\pi} \frac{d\alpha}{\sqrt{[r - a\cos(\alpha)]^2 + a^2\sin^2\alpha + (z-h)^2}} + \int_0^{2\pi} \frac{d\alpha}{\sqrt{[r - a\cos(\alpha)]^2 + a^2\sin^2\alpha + (z+h)^2}} \right] \quad (17)$$
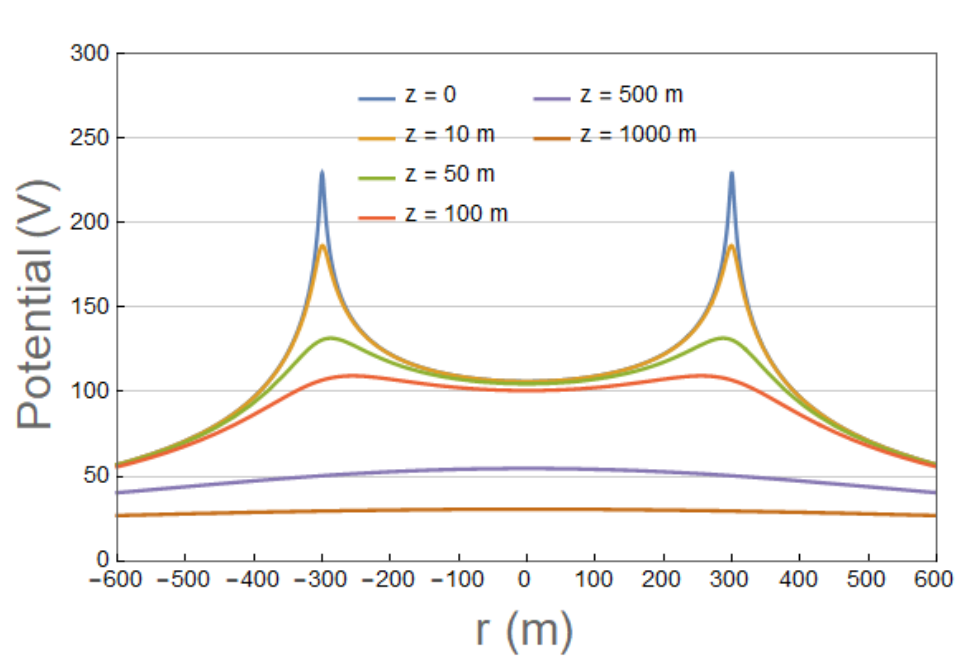
Figure 5 – Potential in the r-direction at different z depths
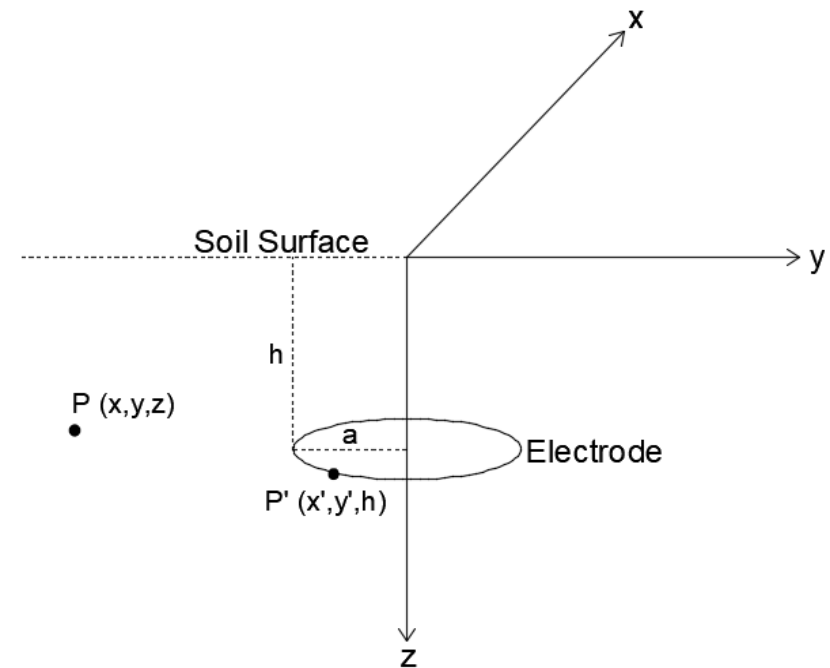
RESULTS

$$J(r,z) = \sqrt{Jr^2 + Jz^2} \qquad (23)$$
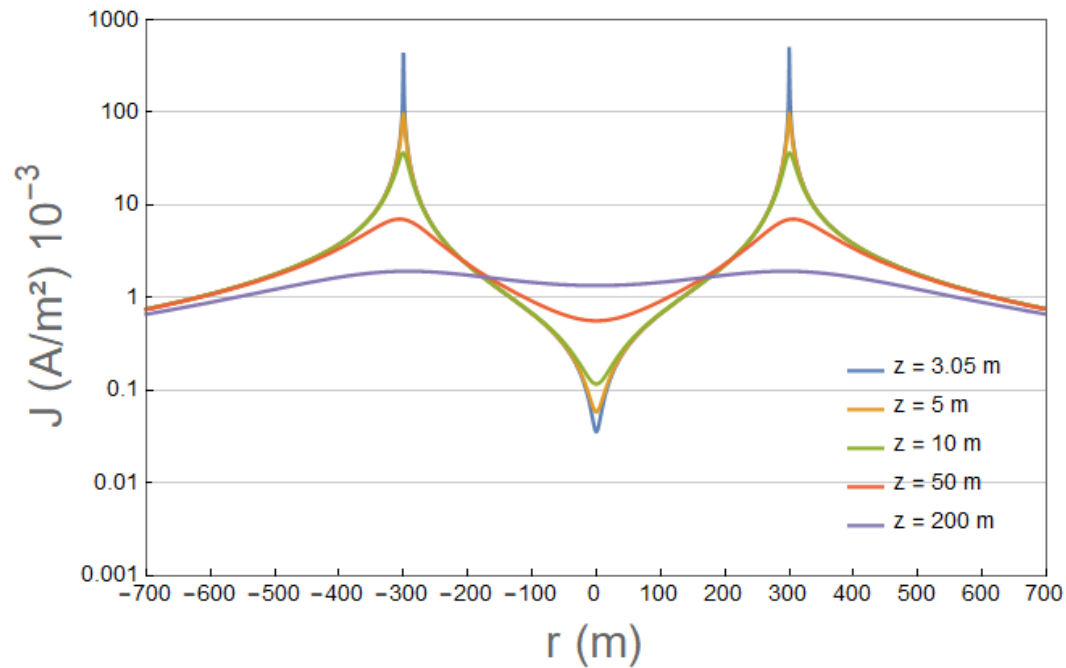
Figure 7 – Current density in the r-direction at different z depths
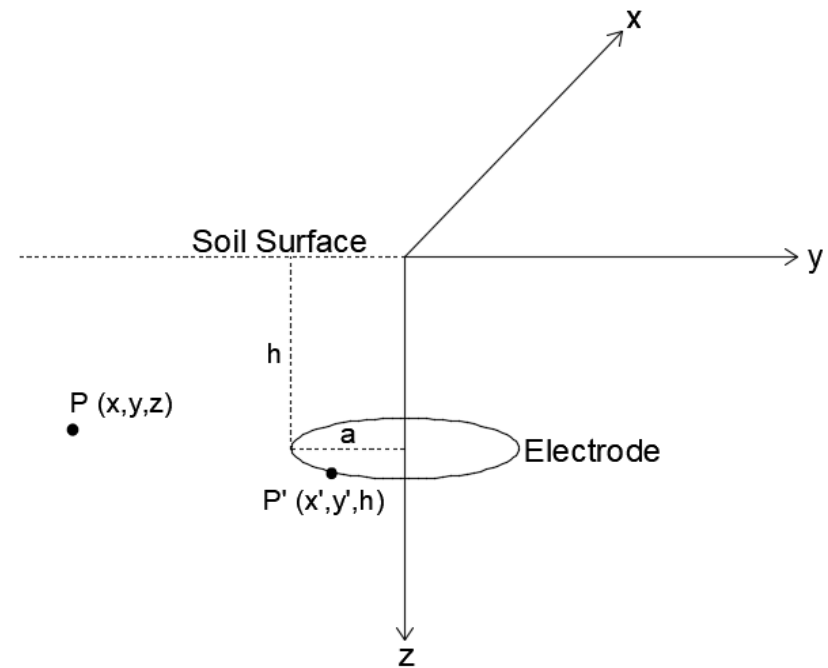
RESULTS

$$\frac{\partial^2 T}{\partial r^2} + \frac{1}{r}\frac{\partial T}{\partial r} + \frac{\partial^2 T}{\partial z^2} + \frac{\rho.J^2}{k} = \frac{1}{\alpha}\frac{\partial T}{\partial t} \qquad (25)$$
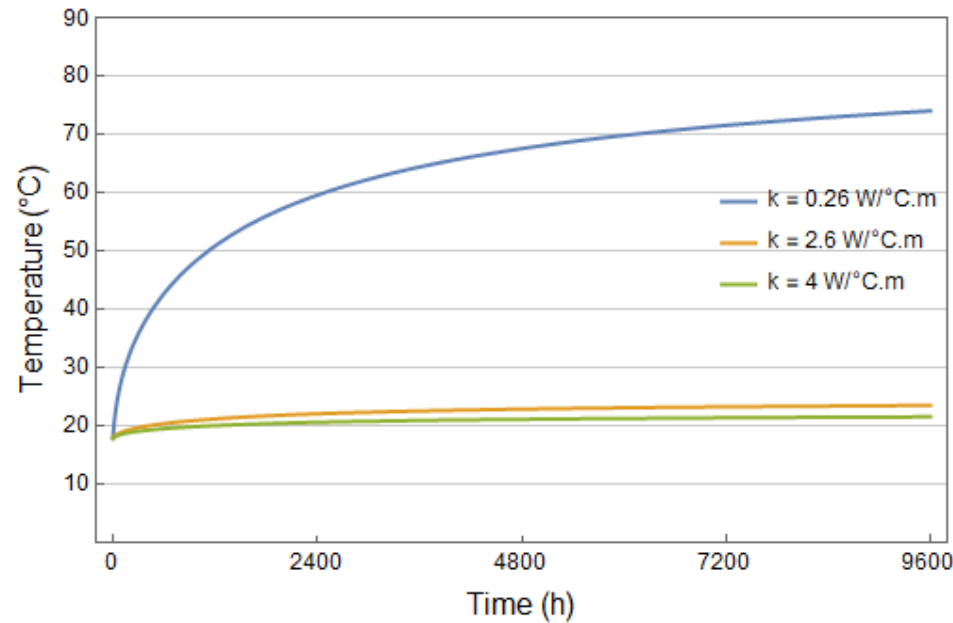
Figure 8 – Temperature increase at the conductor surface (r = 300 m; z = 3 m) after 9600 hours (400 days) of continuous operation
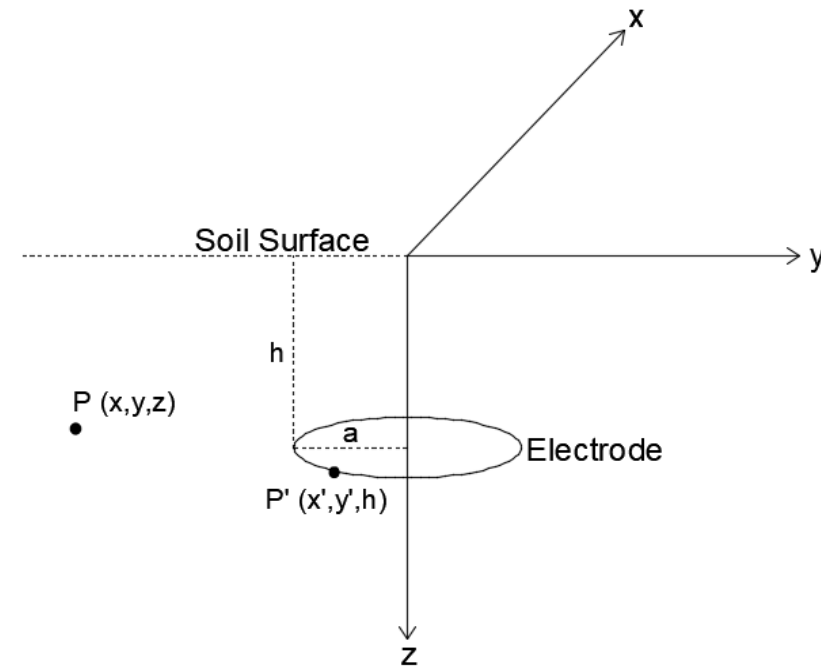
RESULTS

$$\frac{\partial^2 T}{\partial r^2} + \frac{1}{r}\frac{\partial T}{\partial r} + \frac{\partial^2 T}{\partial z^2} + \frac{\rho . J^2}{k} = \frac{1}{\alpha}\frac{\partial T}{\partial t} \qquad (25)$$
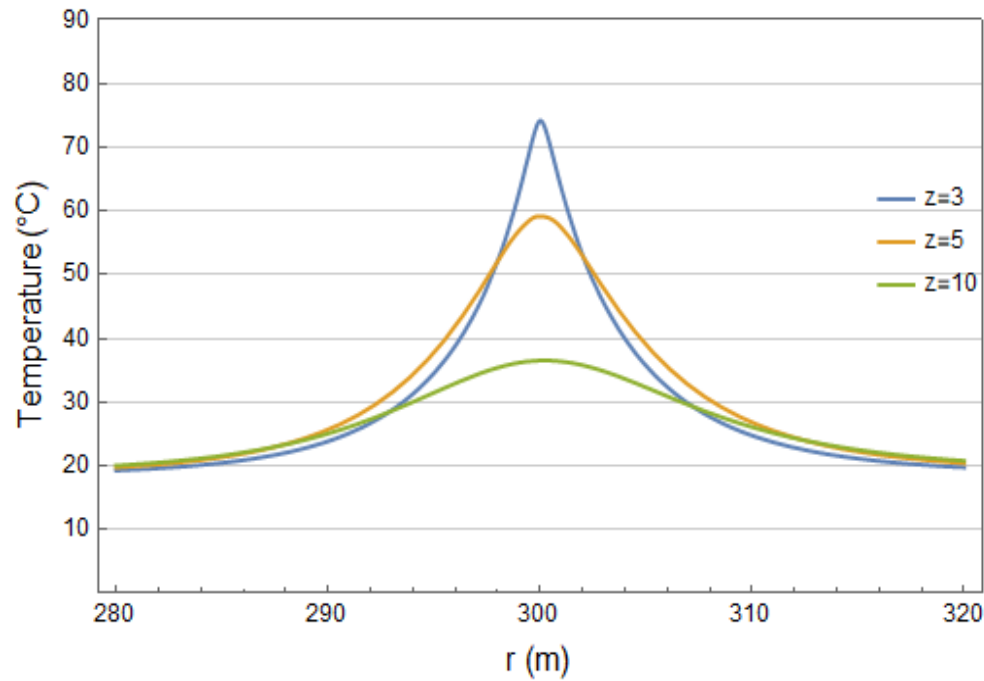
Figure 9 – Temperature distribution in the r-direction at different z depths. k = 0.26 W/°C.m
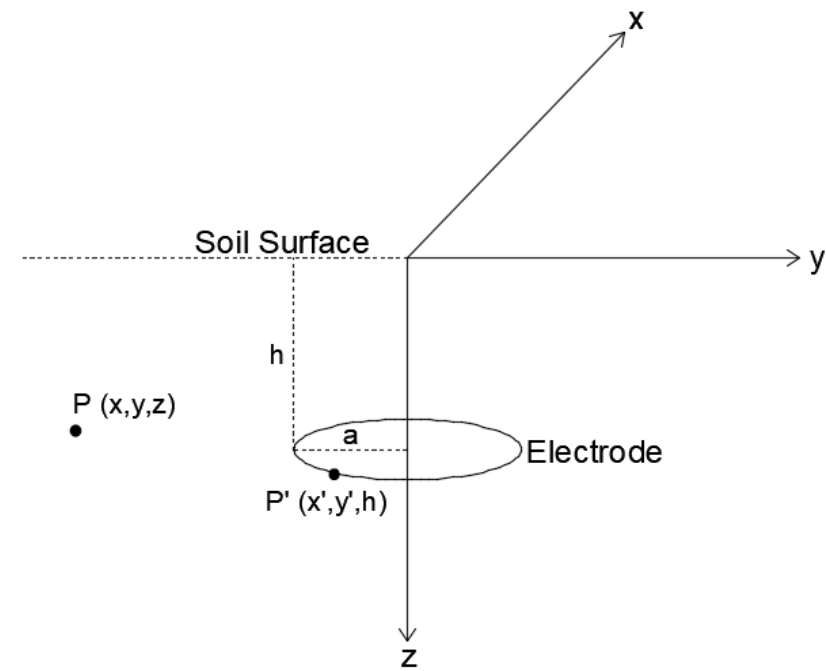
RESULTS

$$\frac{\partial^2 T}{\partial r^2} + \frac{1}{r}\frac{\partial T}{\partial r} + \frac{\partial^2 T}{\partial z^2} + \frac{\rho.J^2}{k} = \frac{1}{\alpha}\frac{\partial T}{\partial t} \qquad (25)$$
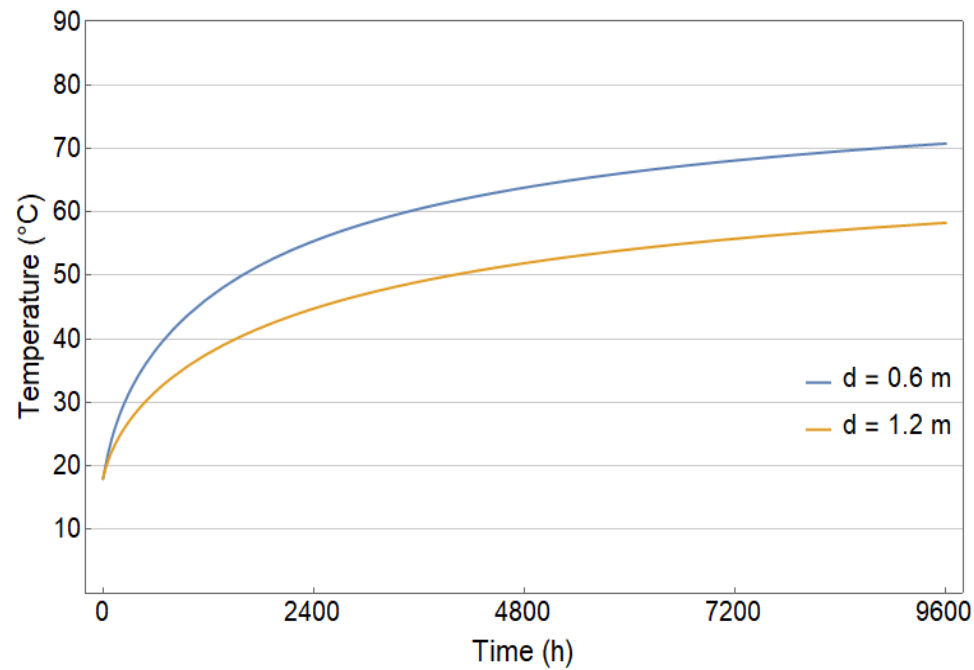
Figure 13 – Temperature increase at r = 300 m and z = 3.5 m after 9600 hours (400 days) of continuous operation considering d = 0.6 m and d = 1.2 m
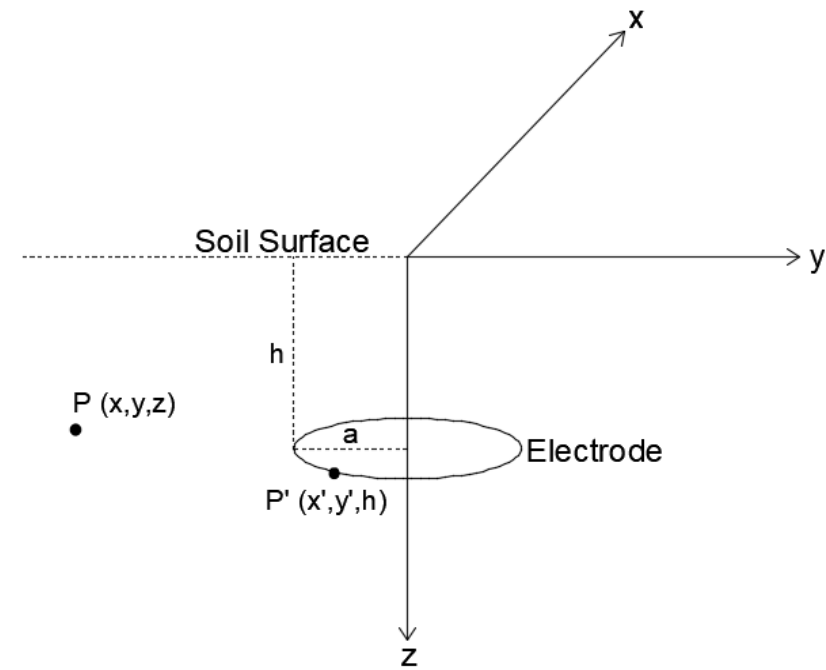
RESULTS

Figure 10 shows how the temperature is distributed in both directions and how important the mechanism of convection is at the soil surface, as it reduces the temperature at the top of the electrode.
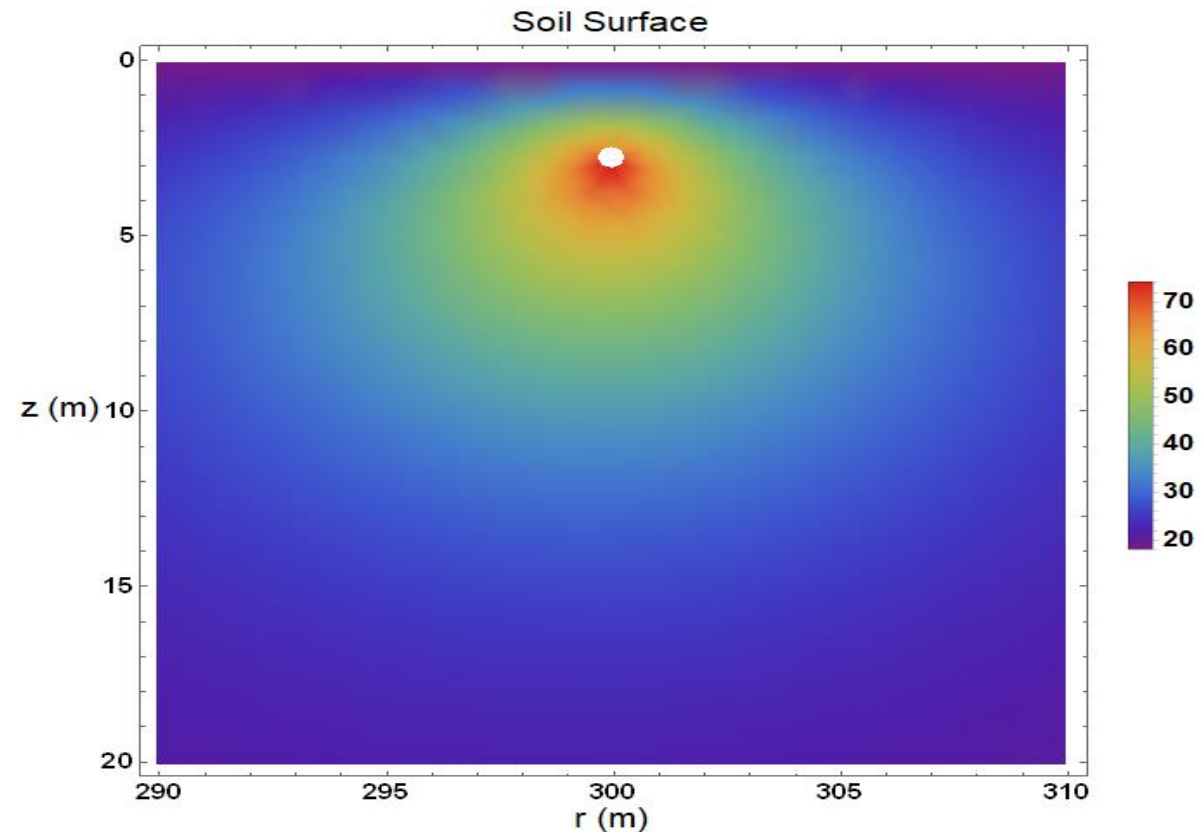
Figure 10 – Temperature distribution along the r and z axes after 9600 hours (400 days) of continuous operation. k = 0.26 W/°C.m

CONTENTS

CONCLUSIONS

- Equations 17 to 23 provide a fast way, in terms of computational time, to verify how the toroidal radius, the depth of burial, the injected current and the soil resistivity affect the voltage, the electric potential, and the current density near the electrode.

- By means of the correct representation of the soil and electrode geometry, and the correct mesh analysis, equation 25 can be easily solved by the finite element method, so the temperature distribution at the electrode vicinity can be calculated in both directions (r and z) and at any time of continuous operation considered.

- As expected, soil temperature is highly affected by the injected current, soil resistivity, thermal conductivity, and the electrode section diameter. The average air temperature also affects the soil temperature, but to a minor degree.

- Variations of thermal diffusivity and convection heat transfer coefficient had little effect on the final soil temperature. However, heat transfer at the surface is dominated by convection, so this mechanism cannot be neglected, or the final temperature of the soil would be much higher.

- The electro-osmosis phenomenon and a n-layered soil were not considered in this paper but must be included in another study, as it is mandatory for a complete analysis of an HVDC ground electrode.

REFERENCES

[1] VILLAS, J.E.T; PORTELA, C.M "Soil Heating Around the Ground Electrode of an HVDC System by Interaction of Electrical, Thermal, and Electroosmotic Phenomena", *IEEE Transactions on Power Delivery,* vol.18, no. 3, July 2003.

[2] H. Greiss, B. L. Allen, P. J. Lagacé, and D. Mukhedkar, "HVDC ground electrode heat dissipation," IEEE Trans. Power Delivery, vol. PWRD-2, pp. 1008–1016, Oct. 1987.

[3] E.W. Kimbark, Direct Current Transmission. New York: Wiley, 1971, pp. 391–473.

[4] VILLAS, J.E.T; PORTELA, C.M "Calculation of Electric Field and Potential Distributions into Soil and Air Media for a Ground Electrode of a HVDC System", *IEEE Transactions on Power Delivery,* vol.18, no. 3, July 2003.

[5] FREIRE, P.E.F.; PANE, EDGAR; "Techniques for the Study of Large Industrial Grounding Systems", *Rio Oil & Gas Expo and Conference 2012 Proceedings*, 2012.

[6] GRAHAM, JOHN.; GUIJUN, LIU, ET AL; "Metodologia de Dimensionamento de Eletrodos Marinhos em Sistemas CCAT", *XXIV Seminário Nacional de Produção e Transmissão de Energia Elétrica*, October 2017.

[7] Themag Engenharia LTDA, HVDC Converter Stations for Voltages Above 600 kV. São Paulo: EPRI, 1985.

REFERENCES

[8] José Antônio Jardini et al, Transmissão em Ultra Alta Tensão em Corrente Alternada. Brasília: Teixeira Gráfica e Editora LTDA, 2017.

[9] Edson H. Watanabe et al., Multi-Infeed HVDC in the Brazilian Interconnected Power System. Brasília: Teixeira Gráfica e Editora LTDA, 2023.

[10] HAMZEHBAHMANI, H; GRIFFITHS, H, ET AL; "Earth Requirements for HVDC Systems", *IEEE*, 2015.

[11] ZOU, J; LIU, Y. Q., ET AL; "Analysis of the Toroidal HVDC Grounding Systems in Horizontal Multilayer Soils", *IEEE*, 2006.

[12] FREIRE, P. EDMUNDO, ET AL; "Sistema de Transmissão HVDC do Rio Madeira-Bipolo 1...", *XXIII Seminário Nacional de Produção e Transmissão de Energia Elétrica*, October 2015.

[13] NOGUEIRA, ROBERTO, ET AL; "Linha de Eletrodo Conversora Terminal Rio UHVDC $\pm$800kV...", *XXV Seminário Nacional de Produção e Transmissão de Energia Elétrica*, November 2019.

[14] ZERBATI, PAULO A., ET AL; "Filosofia de Aplicação e o Estado da Arte da Proteção Elétrica dos Sistemas HVDC-LCC...", *XXVI Seminário Nacional de Produção e Transmissão de Energia Elétrica*, May 2022.

[15] Chan-Ki Kim et al, HVDC Transmission: Power Conversion Applications in Power Systems. Singapore: Wiley, 2009.

CONTENTS

1 – Introduction

2 – Electric Parameters

3 – Heat Conduction

4 – Finite Element Method

5 – Results

6 – Conclusions

7 - References

PURPOSE

To present a distinct formulation to represent the electrothermal phenomena associated with HVDC ring electrodes.

Obrigado!